Understanding Spatiotemporal Photocarrier Dynamics in Monolayer and Bulk MoTe₂ for Optimized Optoelectronic Devices

Shudi Pan,[†] Weijin Kong,[†] Jianhua Liu,[†] Xiaohui Ge,[†] Peymon Zereshki,[‡] Shengcai Hao,[¶] Dawei He,[¶] Yongsheng Wang,[¶] and Hui Zhao*,[‡]

†College of Physics, Qingdao University, Qingdao, Shandong 266071, China.

‡Department of Physics and Astronomy, The University of Kansas, Lawrence, Kansas
66045, United States

¶Key Laboratory of Luminescence and Optical Information, Ministry of Education,
Institute of Optoelectronic Technology, Beijing Jiaotong University, Beijing 100044, China

E-mail: huizhao@ku.edu

Abstract

Semiconducting molybdenum ditelluride has emerged as a promising transition metal dichalcogenide with a number of novel properties. In particular, its bandgap in infrared range makes it an attractive candidate for ultrathin and high-performance infrared optoelectronic applications. Dynamical properties of photocarriers play a key role in determining performance of such devices. We report an experimental study on spatiotemporal dynamics of photocarriers in both monolayer and bulk $MoTe_2$. Transient absorption measurement in reflection geometry revealed ultrafast thermalization and relaxation processes of photocarriers and lifetimes of about 60 and 80 ps in monolayer and bulk $MoTe_2$, respectively. By spatially resolved transient absorption measurements on monolayer, we obtained an exciton diffusion coefficient of $20 \pm 10 \text{ cm}^2$

 $\rm s^{-1}$, a mean free time of 200 fs, a mean free path of 20 nm, and a diffusion length of 350 nm. The corresponding values for the bulk sample are $40 \pm 10 \rm \ cm^2 \ s^{-1}$, 400 fs, 40 nm, and 570 nm, respectively. These results provide fundamental information for understanding and optimizing performance of MoTe₂- based optoelectronic devices.

KEYWORDS: two-dimensional material, transition metal dichalcogenide, molybdenum ditelluride, transient absorption, photocarrier dynamics, exciton, diffusion

Introduction

The discovery of graphene has created an exponentially growing interest in two-dimensional (2D) materials, especially transition metal dichalcogenides (TMDs). Although early efforts have mostly focused on MoS₂ and WS₂, ¹ other members of TMD family have gain significant momentum recently. MoTe₂ with a 2H structure (i.e. 2 layers per hexagonal unit cell) is one type of semiconducting TMD with some unique properties that are complementary to others. Monolayer (ML) MoTe₂ is a direct semiconductor with an optical bandgap of about 1.1 eV.²⁻⁴ Hence, it can extend optoelectronic applications of TMDs to the infrared range. Unlike most TMDs that become indirect in multilayer forms, MoTe₂ retains its direct nature in bilayers.³ MoTe₂ also possesses several other elusive properties such as giant and tunable valley degeneracy splitting,⁵ strong spin-polarization effects,⁶ tunable magnetoresistance,⁷ and metal-semiconductor phase transition.⁸⁻¹¹ The promising charge transport properties make MoTe₂ an attractive candidate for electronic applications such as field-effect transistors.¹²⁻¹⁴ For optoelectronic applications, MoTe₂ photodetectors,^{15,16} light-emitting diodes,¹⁶ and lasers¹⁷ have been demonstrated.

In optoelectronic devices, the dynamical properties of photocarriers, such as their energy relaxation, recombination, and real-space diffusion, are key factors determining device performances. Hence, in developing optoelectronic materials, understanding their photocarrier dynamics is essential. However, in contrast to the extensive efforts reviewed above, studies on photocarrier dynamics in MoTe₂ are rare. In this paper, we report a study on spatiotemporal dynamics of photocarriers in both ML and bulk forms of MoTe₂ by performing spatially and temporally resolved transient absorption measurements. We obtained key parameters describing photocarrier dynamics, including lifetime, diffusion coefficient, mean-free path, and diffusion length, in monolayer and bulk MoTe₂. These results provide fundamental information that is useful for understanding and optimizing performance of MoTe₂-based devices.

Experimental Methods

The MoTe₂ ML samples were fabricated by mechanical exfoliation technique. First, MoTe₂ flakes were peeled off a bulk crystal by an adhesive tape and then transferred onto a polydimethylsiloxane (PDMS) substrate. We used optical contrast to identify ML regions. It has been established that for a thin layer on a thick and transparent substrate, the optical contrast is approximately proportional to the thickness of the thin layer. ^{2,18–20} The green channel contrasts of the flakes containing regions of different thicknesses show clear step-like behavior, with the step of about 0.25 corresponding to MLs. No contrast lower than this level was observed. This result is also consistent with the previously reported contrast of ML MoTe₂.² One ML flake identified was transferred to a Si/SiO₂ substrate. A multilayer hexagonal boron nitride (h-BN), obtained by the same exfoliation procedure, was immediately transferred on top of $MoTe_2$ as a protective layer. The sample was thermally annealed at 200°C for 2 hours under a H₂-Ar (20-100 sccm) environment at a base pressure of about 3 Torr. Due to the protection of the top h-BN layer, no sample degradation was noticed during the entire course of the study. An optical microscope image of the sample used in this study is shown in Figure 1(a). We note that because of the h-BN layer, atomic force microscopy and Raman measurements are less effective in determining the thickness of MoTe₂.

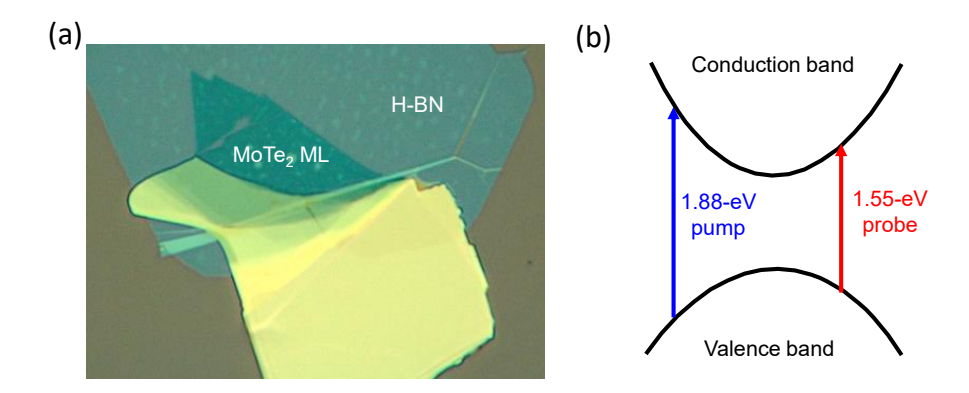


Figure 1: (a) Optical microscope image of the MoTe₂ monolayer sample covered by an h-BN layer for protection. (b) Schematics of pump-probe configuration.

Photocarrier dynamics in MoTe₂ was studied by transient absorption technique in reflection geometry. ²¹ The transient absorption setup used an 80-MHz Ti:sapphire laser system. The 800-nm (1.55 eV) and 100-fs output was split into two parts. One part was directly used in the measurement as the probe pulse. The fluence of this pulse was about 0.2 μ J cm⁻². The other part was sent to a photonic crystal fiber, from which a broadband supercontinuum was obtained. A bandpass filter with a 10-nm bandwidth was used to select a component centered at 660 nm (1.88 eV), which was used as the pump pulse. Its fluence was in the range of 2 - 10 μ J cm⁻², controlled by a half-wave plate followed by a polarizer. The two pulses were combined by a beamsplitter and focused on the sample by a microscope objective lens with a numerical aperture of 0.4 to a spot size of about 2 μ m. The reflected probe beam was measured by a photodiode and a lock-in amplifier. All the measurements were performed under ambient condition.

In this configuration, the probe photon energy is significantly higher than the optical bandgap of MoTe₂. Using the infrared part of the suprecontiunuum as the probe could potentially enhance the signal; however, its intensity noise is much higher than the 1.55-eV beam since it is produced by the latter through a nonlinear process. The longer wavelength would also result in a larger spot size and thus poorer spatial resolution. Hence, the chosen configuration, although not ideal, is suitable for the purpose of this study.

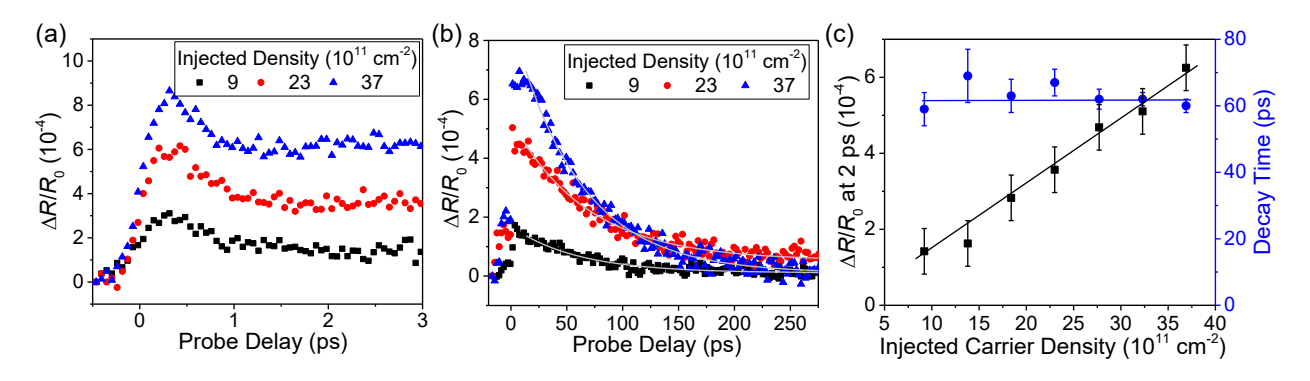


Figure 2: (a) Differential reflection of MoTe₂ monolayer as a function of probe delay with injected photocarrier densities of 9 (black), 23 (red), and 37×10^{11} cm⁻² (blue), respectively. (b) Same as (a) but for a larger delay range. The light-gray curves over the data are exponential fits. (c) The differential reflection signal with a probe delay of 2 ps (black squares, left axis) and the decay time constant obtained from the exponential fits (blue circles, right axis) as a function of the injected carrier density.

Results and Discussion

We time resolved photocarrier dynamics in the MoTe₂ ML sample by using the pump-probe scheme illustrated in Figure 1(b). The 1.88-eV pump excites photocarriers in the form of electron-hole pairs by interband transition. With an excitation excess energy of 780 meV, carriers are injected with high kinetic energies. To monitor the dynamics of the injected carriers, differential reflection of the 1.55-eV probe pulse was measured as a function of the probe delay, which is the delay of the arrival time of the probe pulse at the sample with respect to the pump pulse. The differential reflection is defined as the normalized difference between the reflectivity of the probe pulse by the sample with (R) and without (R_0) the presence of the pump pulse, $\Delta R/R_0 = (R-R_0)/R_0$. It can be shown that when $\Delta R/R_0 \ll 1$, this quantity is proportional to the change of the complex index of refraction of the sample by the pump. ²² Since in low-density regimes the absorption change is proportional to the photocarrier density, ²³ the differential reflection can be used to monitor the photocarrier dynamics.

Figure 2 (a) and (b) show the obtained differential reflection signal in short and long time ranges, respectively, for different injected carrier densities. Here, the injected carrier

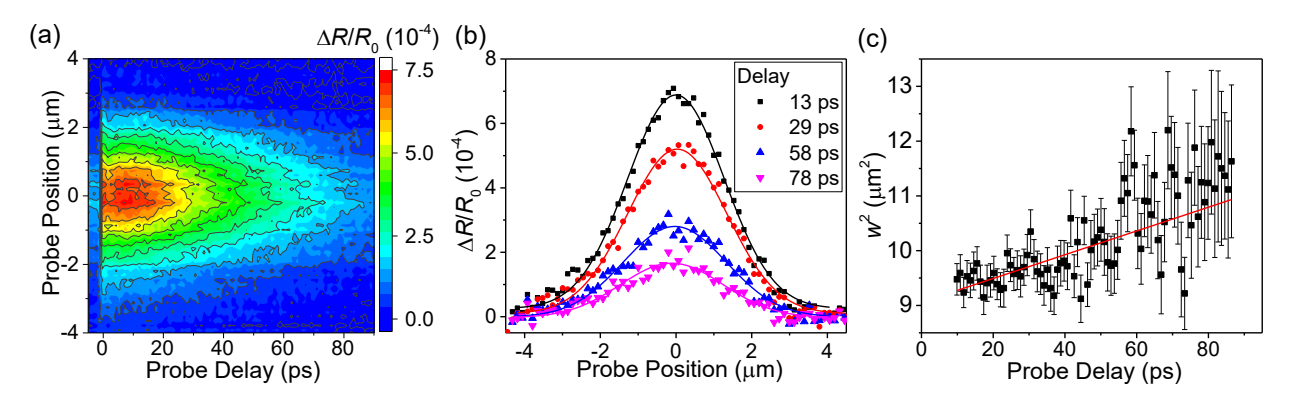


Figure 3: (a) Spatiotemporally resolved differential reflection signal measured from MoTe₂ monolayer. (b) Differential reflection signal as a function of the probe spot position with respect to the pump spot for several probe delays. The curves are Gaussian fits. (c) The square width of the profile, obtained by Gaussian fits, as a function of probe delay. The red line is a linear fit with a diffusion coefficient of 20 cm² s⁻¹.

densities are estimated from the pump fluence used in each scan: 24 Using the absorption coefficient of $3 \times 10^8 \text{ m}^{-1}$ at 1.88 eV in ML MoTe₂² and assuming that every pump photon absorbed generates an electron-hole pair, a pump fluence of 1 μJ cm⁻² corresponds to an injected photocarrier density of $6.2 \times 10^{11} \text{ cm}^{-2}$. We find that the differential reflection signal reaches a peak on a time range limited by the instrument response time of about 350 fs. This indicates that the nonequilibrium carriers injected by the 1.88-eV pump thermalize and relax their kinetic energy to reach the states monitored by the 1.55-eV probe on an ultrafast time scale. This is consistent with observations of ultrafast thermalization and energy relaxation of photocarriers in other TMD monolayers, such as MoS_2 , 22 $MoSe_2$, 25,26 $\mathrm{WS}_2,^{27}$ and $\mathrm{WSe}_2,^{28}$ and can be attributed to the enhanced carrier-carrier scattering and carrier-phonon scattering due to the reduction of dielectric screening. After the peak, the signal decay by about 20 - 30 % in about 400 fs. This can be attributed to the evolution of carrier distribution from the states probed by the 1.55-eV pulse to the bandedges. After these fast processes, the carriers are expected to form a thermal distribution with a temperature equals to the lattice temperature, which is 300 K, and form excitons. ²⁹ The signal at 2 ps is proportional to the injected density, as shown by the black squares in Figure 2(c). This ensures that the evolution of the differential reflection truly reflects variation of the carrier density. The long-term decay of the signal can be fit by single-exponential functions, as shown by the light-gray curves in Figure 2(b). The obtained decay constant reflects the lifetime of excitons, which is about 60 ps and is independent of the carrier density in the range studied here, as shown by the blue circles in Figure 2(c). This shows that the exciton recombination is a single-molecule process and multiple-exciton processes ^{30,31} play a minor role under these conditions. We note that the peak signal seen in (b) is lower than (a) because the peak in (a) was not captures in this scan with a larger step size.

To study diffusion of excitons in MoTe₂ ML, we performed spatially resolved differential reflection measurements. By tilting a mirror in the probe arm, we can move the probe laser spot and thus vary the distance between the centers of the pump and probe spots. By scanning the probe spot along the horizontal direction and measuring the differential reflection signal as a function of the probe delay for each probe position, we obtained the differential reflection signal as a function of both probe delay and probe position, as shown in Figure 3(a). At each probe delay, the spatial profile of the signal is close to a Gaussian function. Figure 3(b) shows some examples of the profiles with the Gaussian fits (curves). From the fit to each profile measured, we obtained the full width at half maximum (w) of each profile. The squared width, w^2 , is plotted in Figure 3(c) as a function of the probe delay. Despite of the large uncertainty of the data limited by the signal-to-noise ratio, we can clearly observe a trend of broadening of the profile up to about 50 ps, indicating an expansion of the exciton density profile. After 50 ps, due to a lower signal-to-noise ratio, the expansion is uncertain.

The expansion of the exciton density profile is induced by exciton in-plane diffusion driven by the density gradient. This process is described by the diffusion equation. It can be shown that for initial Gaussian density profile, the width of the profile expands as $w^2 = w_0^2 + 11.09Dt$, where w_0 is the initial width and D, the diffusion coefficient of the excitons.³² With a linear fit to the squared width in Figure 3(c), we find a diffusion coefficient of about $20 \pm 10 \text{ cm}^2/\text{s}$. We note that in the above analysis, we did not consider

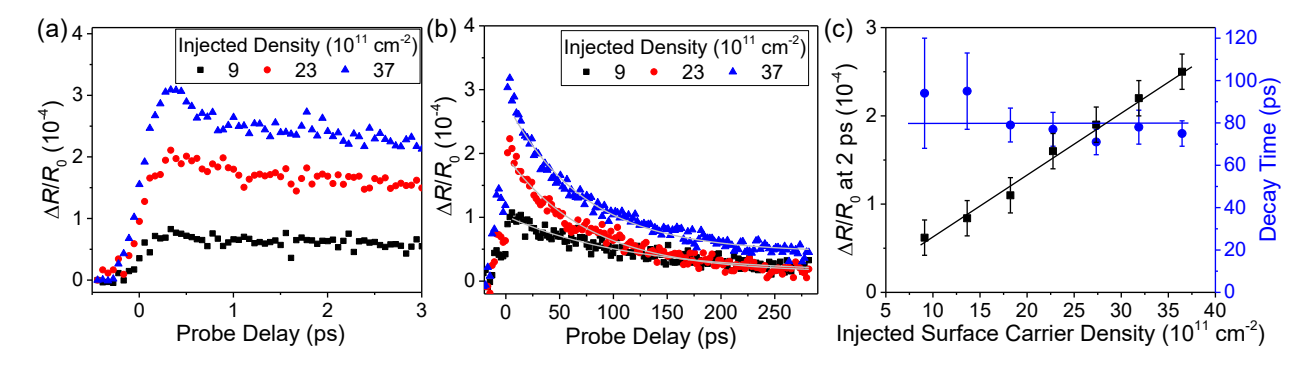


Figure 4: (a) Differential reflection of MoTe₂ bulk as a function of probe delay with injected photocarrier densities at the sample surface of 9 (black), 23 (red), and 37×10^{11} cm⁻² (blue), respectively. (b) Same as (a) but for a larger delay range. The light-gray curves over the data are exponential fits. (c) The differential reflection signal with a probe delay of 2 ps (black squares, left axis) and the decay time constant obtained from the exponential fits (blue circles, right axis) as a function of the injected carrier density.

the finite size of the probe spot. In the measurement, the pump and probe spots are similar sizes and hence the measured profile is the convolution of the actual exciton density (the pump intensity profile) and the probe intensity profile. Since both spots are Gaussian, the convoluted square width is the sum of the square widths of the exciton density and the probe intensity profiles. Since the probe intensity profile does not change with probe delay, it merely adds a constant to both sides of the equation used to obtain the diffusion coefficient.³³

Exciton diffusion is a thermal motion limited by scattering; hence, the diffusion coefficient reveals the microscopic interaction of excitons with their environment. At room temperature, thermal speed of excitons in 2D, $v_T = \sqrt{2k_BT/m_X}$, is about 10^5 m s⁻¹ using an exciton effective mass of $m_X \approx 10^{-32}$ kg.³⁴ Hence, the measured diffusion coefficient indicates a mean free time of $D/v_T^2 \approx 200$ fs, or a momentum relaxation rate of 5×10^{12} s⁻¹. The mean free path of excitons is about 20 nm. Furthermore, by using the measured exciton lifetime of 60 ps, we obtain a diffusion length of $\sqrt{D\tau} = 350$ nm.

For comparison, we also studied photocarrier dynamics in bulk MoTe₂ under the same experimental conditions. The same crystal used to fabricate the ML sample was used to rule out potential impacts of sample variations. Figure 4 summarized the results obtained from the bulk sample in a similar fashion as Figure 2. Due to the small penetration depth of

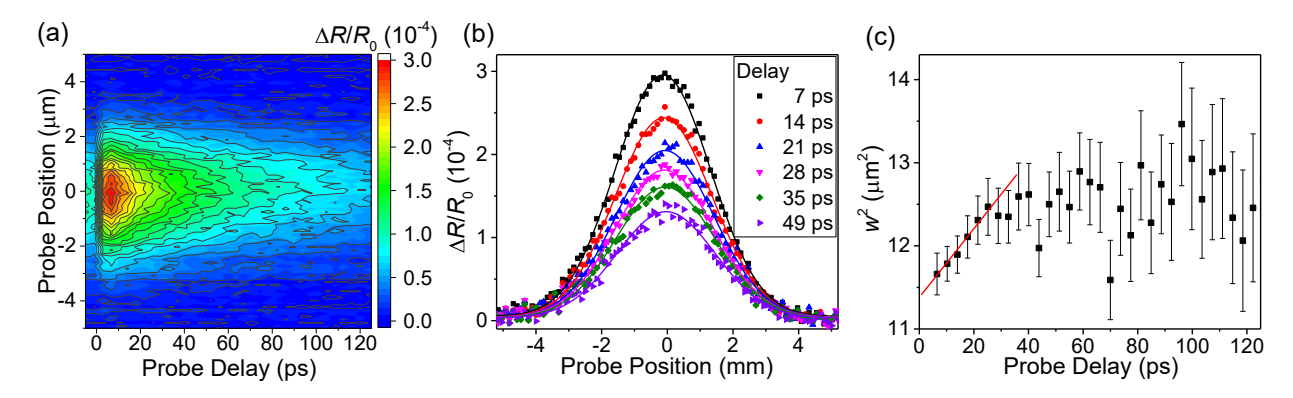


Figure 5: (a) Spatiotemporally resolved differential reflection signal measured from the MoTe₂ bulk sample. (b) Differential reflection signal as a function of the probe spot position with respect to the pump spot for several probe delays. The curves are Gaussian fits. (c) The square width of the profile, obtained by Gaussian fits, as a function of probe delay. The red line is a linear fit with a diffusion coefficient of 40 cm² s⁻¹.

MoTe₂ of only a few nanometers, the 1.88-eV pump only excite a few layers of the sample. The carrier density shown in Figure 4 represents the density in the first layer of MoTe₂. We find that the magnitude of the signal in bulk is still proportional to carrier density and is smaller than ML by a factor of 2. This can be attributed to two effects: First, the probe access energy is higher than in ML since the bandgap of bulk MoTe₂ is smaller. Hence, the probing efficiency is expected to reduce. Second, since several layers are excited, the effect areal carrier density is smaller. The initial fast decay component observed in ML is less pronounced in bulk, suggesting different carrier dynamics in early stage. The lifetime of excitons in bulk is found to be about 80 ps, which is slightly longer than ML and also independent of the carrier density.

Exciton diffusion in bulk MoTe₂ was studied with the same spatially resolved measurements. The results are summarized in Figure 5. The diffusion appears to persist for about 40 ps. A linear fit to the data in the first 40 ps results in a diffusion coefficient of about 40 \pm 10 cm² s⁻¹, which is about twice larger than ML. After this phase, the profile appears to be steady. Considering the majority of injected excitons have recombined in the first 40 ps, this effect could be attributed to trapping of residual excitons by impurities. From the diffusion coefficient and lifetime, we also deduce a mean free time of about 400 fs, a momentum

relaxation rate of $2.5 \times 10^{12}~\rm s^{-1}$, a mean free path of 40 nm, and a diffusion length of 570 nm. In the bulk sample, excitons also diffuse vertically. In our analysis, this process was not considered for two reasons. First, only the in-plane areal density of excitons is measured by the differential reflection. Hence, our technique is less sensitive to the vertical diffusion. Second, as a layered structure, the vertical (interlayer) diffusion coefficient is expected to be much smaller than in-plane diffusion coefficient, and hence its effect to our analysis is negligible.

Finally, from the measured diffusion coefficients, we can deduce the exciton mobilities for ML and bulk MoTe₂ using Einstein relation, $D/k_BT = \mu/e$, where k_B , T, and μ are the Boltzmann constant, the exciton temperature, and the mobility. We obtain exciton mobilities on the order of 700 and 1,400 cm² V⁻¹ s⁻¹ for ML and bulk, respectively. Recent experimental studies have achieved room-temperature charge-carrier mobilities in the range of 10 - 100 cm² V⁻¹ s⁻¹ for MoTe₂, ^{35–38} while theoretical values of about 2,500 cm² V⁻¹ s⁻¹ has been predicted. ³⁴ The larger values of exciton mobility can be attributed to the fact that excitons are neutral quasiparticles. Compared to charged carriers, their interaction with charged impurities and phonons is weaker, resulting in a higher mobility. Indeed, the trend of exciton mobility being higher than charge mobility has been observed in other types of 2D materials. ^{22,25,27,28,39,40}

Conclusions

We have studied photocarrier dynamics in both monolayer and bulk samples of MoTe₂. We obtained an exciton lifetime of about 60 ps and an exciton diffusion coefficient of about 20 cm² s⁻¹ in the monolayer sample fabricated by mechanical exfoliation. In bulk, these parameters were found to be 80 ps and 40 cm² s⁻¹. These results provide quantitative description of excitonic dynamics in MoTe₂, which is important for understanding and optimizing performance of optoelectonic devices based on MoTe₂. For example, the exciton

lifetime is an important parameter determining power conversion efficiency of photovoltaic devices, response time of photodetectors, and quantum efficiency of light-emitting devices. The diffusion process is an important consideration when designing lateral electronic and energy devices. Furthermore, the mean free time and mean free path reveals fundamental properties of excitons and their interaction with phonons.

Acknowledgement

This material is based upon work supported by Shandong Province Natural Science Foundation (Project ZR2014FM037), National Nature Science Foundation of China (Project 11274188), and National Science Foundation of USA (DMR-1505852).

References

- Lin, Z.; McCreary, A.; Briggs, N.; Subramanian, S.; Zhang, K. H.; Sun, Y. F.; Li, X. F.; Borys, N. J.; Yuan, H. T.; Fullerton-Shirey, S. K.; Chernikov, A.; Zhao, H.; McDonnell, S.; Lindenberg, A. M.; Xiao, K.; LeRoy, B. J.; Drndic, M.; Hwang, J. C. M.; Park, J.; Chhowalla, M.; Schaak, R. E.; Javey, A.; Hersam, M. C.; Robinson, J.; Terrones, M. 2D Materials Advances: From Large Scale Synthesis and Controlled Heterostructures to Improved Characterization Techniques, Defects and Applications. 2D Mater. 2016, 3, 042001.
- (2) Ruppert, C.; Aslan, O. B.; Heinz, T. F. Optical Properties and Band Gap of Single-and Few-Layer MoTe₂ Crystals. *Nano Lett.* **2014**, *14*, 6231–6236.
- (3) Lezama, I. G.; Arora, A.; Ubaldini, A.; Barreteau, C.; Giannini, E.; Potemski, M.; Morpurgo, A. F. Indirect-to-Direct Band Gap Crossover in Few-Layer MoTe₂. Nano Lett. 2015, 15, 2336–2342.

- (4) Yang, J.; Lu, T.; Myint, Y. W.; Pei, J.; Macdonald, D.; Zheng, J. C.; Lu, Y. Robust Excitons and Trions in Monolayer MoTe₂. ACS Nano **2015**, 9, 6603–6609.
- (5) Qi, J. S.; Li, X.; Niu, Q.; Feng, J. Giant and Tunable Valley Degeneracy Splitting in MoTe₂. Phys. Rev. B **2015**, 92, 121403.
- (6) Zhang, Q. Y.; Yang, S. Y. A.; Mi, W. B.; Cheng, Y. C.; Schwingenschlogl, U. Large Spin-Valley Polarization in Monolayer MoTe₂ on Top of EuO(111). Adv. Mater. 2016, 28, 959–966.
- (7) Yang, J. J.; Colen, J.; Liu, J.; Nguyen, M. C.; Chern, G. W.; Louca, D. Elastic and Electronic Tuning of Magnetoresistance in MoTe₂. Sci. Adv. **2017**, 3, eaao4949.
- (8) Cho, S.; Kim, S.; Kim, J. H.; Zhao, J.; Seok, J.; Keum, D. H.; Baik, J.; Choe, D. H.; Chang, K. J.; Suenaga, K.; Kim, S. W.; Lee, Y. H.; Yang, H. Device Technology Phase Patterning for Ohmic Homojunction Contact in MoTe₂. Science **2015**, 349, 625–628.
- (9) Keum, D. H.; Cho, S.; Kim, J. H.; Choe, D. H.; Sung, H. J.; Kan, M.; Kang, H.; Hwang, J. Y.; Kim, S. W.; Yang, H.; Chang, K. J.; Lee, Y. H. Bandgap Opening in Few-Layered Monoclinic MoTe₂. Nat. Phys. 2015, 11, 482–487.
- (10) Sung, J. H.; Heo, H.; Si, S.; Kim, Y. H.; Noh, H. R.; Song, K.; Kim, J.; Lee, C. S.; Seo, S. Y.; Kim, D. H.; Kim, H. K.; Yeom, H. W.; Kim, T. H.; Choi, S. Y.; Kim, J. S.; Jo, M. H. Coplanar Semiconductor-Metal Circuitry Defined on Few-Layer MoTe₂ via Polymorphic Heteroepitaxy. Nat. Nanotechnol. **2017**, 12, 1064–1070.
- (11) Wang, Y.; Xiao, J.; Zhu, H. Y.; Li, Y.; Alsaid, Y.; Fong, K. Y.; Zhou, Y.; Wang, S. Q.; Shi, W.; Wang, Y.; Zettl, A.; Reed, E. J.; Zhang, X. Structural Phase Transition in Monolayer MoTe₂ Driven by Electrostatic Doping. *Nature* 2017, 550, 487–491.
- (12) Fathipour, S.; Ma, N.; Hwang, W. S.; Protasenko, V.; Vishwanath, S.; Xing, H. G.;

- Xu, H.; Jena, D.; Appenzeller, J.; Seabaugh, A. Exfoliated Multilayer MoTe₂ Field-Effect Transistors. *Appl. Phys. Lett.* **2014**, *105*, 192101.
- (13) Pradhan, N. R.; Rhodes, D.; Feng, S.; Xin, Y.; Memaran, S.; Moon, B. H.; Terrones, H.; Terrones, M.; Balicas, L. Field-effect transistors based on few-layered α-MoTe₂. ACS Nano 2014, 8, 5911–5920.
- (14) Chang, Y. M.; Yang, S. H.; Lin, C. Y.; Chen, C. H.; Lien, C. H.; Jian, W. B.; Ueno, K.; Suen, Y. W.; Tsukagoshi, K.; Lin, Y. F. Reversible and Precisely Controllable P/N-Type Doping of MoTe₂ Transistors through Electrothermal Doping. Adv. Mater. 2018, 30, 1706995.
- (15) Zhang, K. A.; Zhang, T. N.; Cheng, G. H.; Li, T. X.; Wang, S. X.; Wei, W.; Zhou, X. H.; Yu, W. W.; Sun, Y.; Wang, P.; Zhang, D.; Zeng, C. G.; Wang, X. J.; Hu, W. D.; Fan, H. J.; Shen, G. Z.; Chen, X.; Duan, X. F.; Chang, K.; Dai, N. Interlayer Transition and Infrared Photodetection in Atomically Thin Type-II MoTe₂/MoS₂ van der Waals Heterostructures. ACS Nano 2016, 10, 3852–3858.
- (16) Bie, Y. Q.; Grosso, G.; Heuck, M.; Furchi, M. M.; Cao, Y.; Zheng, J. B.; Bunandar, D.; Navarro-Moratalla, E.; Zhou, L.; Efetov, D. K.; Taniguchi, T.; Watanabe, K.; Kong, J.; Englund, D.; Jarillo-Herrero, P. A MoTe₂-Based Light-Emitting Diode and Photodetector for Silicon Photonic Integrated Circuits. *Nat. Nanotechnol.* 2017, 12, 1124–1129.
- (17) Li, Y. Z.; Zhang, J. X.; Huang, D. D.; Sun, H.; Fan, F.; Feng, J. B.; Wang, Z.; Ning, C. Z. Room-Temperature Continuous-Wave Lasing from Monolayer Molybdenum Ditelluride Integrated with a Silicon Nanobeam Cavity. Nat. Nanotechnol. 2017, 12, 987–992.
- (18) Ceballos, F.; Zereshki, P.; Zhao, H. Separating Electrons and Holes by Monolayer Increments in van der Waals Heterostructures. *Phys. Rev. Mater.* **2017**, *1*, 044001.

- (19) Cui, Q.; Muniz, R. A.; Sipe, J. E.; Zhao, H. Strong and Anisotropic Third-Harmonic Generation in Monolayer and Multilayer ReS₂. *Phys. Rev. B* **2017**, *95*, 165406.
- (20) Zereshki, P.; Wei, Y. Q.; Ceballos, F.; Bellus, M. Z.; Lane, S. D.; Pan, S. D.; Long, R.; Zhao, H. Photocarrier Dynamics in Monolayer Phosphorene and Bulk Black Phosphorus. Nanoscale 2018, 10, 11307–11313.
- (21) Ceballos, F.; Zhao, H. Ultrafast Laser Spectroscopy of Two-Dimensional Materials beyond Graphene. Adv. Funct. Mater. 2017, 27, 1604509.
- (22) Wang, R.; Ruzicka, B. A.; Kumar, N.; Bellus, M. Z.; Chiu, H.-Y.; Zhao, H. Ultrafast and Spatially Resolved Studies of Charge Carriers in Atomically Thin Molybdenum Disulfide. *Phys. Rev. B* **2012**, *86*, 045406.
- (23) Schmitt-Rink, S.; Chemla, D. S.; Miller, D. A. B. Theory of Transient Excitonic Optical Nonlinearities in Semiconductor Quantum-Well Structures. *Phys. Rev. B* **1985**, *32*, 6601–6609.
- (24) Ceballos, F.; Ju, M. G.; Lane, S. D.; Zeng, X. C.; Zhao, H. Highly Efficient and Anomalous Charge Transfer in van der Waals Trilayer Semiconductors. *Nano Lett.* **2017**, *17*, 1623–1628.
- (25) Kumar, N.; Cui, Q.; Ceballos, F.; He, D.; Wang, Y.; Zhao, H. Exciton diffusion in monolayer and bulk MoSe₂. Nanoscale **2014**, 6, 4915–4919.
- (26) Kumar, N.; He, J.; He, D.; Wang, Y.; Zhao, H. Valley and spin dynamics in MoSe₂ two-dimensional crystals. *Nanoscale* **2014**, *6*, 12690–12695.
- (27) He, J.; He, D.; Wang, Y.; Cui, Q.; Ceballos, F.; Zhao, H. Spatiotemporal Dynamics of Excitons in Monolayer and Bulk WS₂. *Nanoscale* **2015**, *7*, 9526–9531.
- (28) Cui, Q.; Ceballos, F.; Kumar, N.; Zhao, H. Transient absorption microscopy of monolayer and bulk WSe₂. ACS Nano **2014**, 8, 2970–2976.

- (29) Ceballos, F.; Cui, Q.; Bellus, M. Z.; Zhao, H. Exciton Formation in Monolayer Transition Metal Dichalcogenides. *Nanoscale* **2016**, *8*, 11681–11688.
- (30) Kumar, N.; Cui, Q.; Ceballos, F.; He, D.; Wang, Y.; Zhao, H. Exciton-Exciton Annihilation in MoSe₂ Monolayers. *Phys. Rev. B* **2014**, *89*, 125427.
- (31) Sun, D.; Rao, Y.; Reider, G. A.; Chen, G.; You, Y.; Brezin, L.; Harutyunyan, A. R.; Heinz, T. F. Observation of Rapid Exciton-Exciton Annihilation in Monolayer Molybdenum Disulfide. *Nano Lett.* **2014**, *14*, 5625–5629.
- (32) Kumar, N.; He, J.; He, D.; Wang, Y.; Zhao, H. Charge carrier dynamics in bulk MoS₂ crystal studied by transient absorption microscopy. *J. Appl. Phys.* **2013**, *113*, 133702.
- (33) Zhao, H. Temperature dependence of ambipolar diffusion in silicon-on-insulator. *Appl. Phys. Lett.* **2008**, *92*, 112104.
- (34) Zhang, W.; Huang, Z.; Zhang, W.; Li, Y. Two-Dimensional Semiconductors with Possible High Room Temperature Mobility. *Nano Res.* **2014**, *7*, 1731–1737.
- (35) Cho, Y.; Park, J. H.; Kim, M.; Jeong, Y.; Ahn, J.; Kim, T.; Choi, H.; Yi, Y.; Im, S. Fully Transparent P-Mote₂ 2D Transistors Using Ultrathin MoO_x/Pt Contact Media for Indium-Tin-Oxide Source/Drain. *Adv. Funct. Mater.* **2018**, *28*, 1801204.
- (36) Qu, D. S.; Liu, X. C.; Huang, M.; Lee, C.; Ahmed, F.; Kim, H.; Ruoff, R. S.; Hone, J.; Yoo, W. J. Carrier-Type Modulation and Mobility Improvement of Thin MoTe₂. Adv. Mater. 2017, 29, 1606433.
- (37) Huang, J. H.; Deng, K. Y.; Liu, P. S.; Wu, C. T.; Chou, C. T.; Chang, W. H.; Lee, Y. J.; Hou, T. H. Large-Area 2D Layered MoTe₂ by Physical Vapor Deposition and Solid-Phase Crystallization in a Tellurium-Free Atmosphere. Adv. Mater. Interfaces 2017, 4, 1700157.

- (38) Lim, J. Y.; Pezeshki, A.; Oh, S.; Kim, J. S.; Lee, Y. T.; Yu, S.; Hwang, D. K.; Lee, G. H.; Choi, H. J.; Im, S. Homogeneous 2D MoTe₂ P-N Junctions and Cmos Inverters Formed by Atomic-Layer-Deposition-Induced Doping. *Adv. Mater.* **2017**, *29*, 1701798.
- (39) Cui, Q.; He, J.; Bellus, M. Z.; Mirzokarimov, M.; Hofmann, T.; Chiu, H.-Y.; Antonik, M.; He, D.; Wang, Y.; Zhao, H. Transient Absorption Measurements on Anisotropic Monolayer ReS₂. Small **2015**, 11, 5565–5571.
- (40) He, J.; He, D.; Wang, Y.; Cui, Q.; Bellus, M. Z.; Chiu, H.-Y.; Zhao, H. Exceptional and Anisotropic Transport Properties of Photocarriers in Black Phosphorus. *ACS Nano* **2015**, *9*, 6436–6442.

Graphical TOC Entry

